

Acoustic Response of Unexploded Ordnance (UXO) and Cylindrical Targets

Steven G. Kargl and Kevin L. Williams
Applied Physics Laboratory
University of Washington
1013 NE 40th St
Seattle WA 98105
Email: kargl@apl.washington.edu

Timothy M. Marston
Physics and Astronomy Dept.
Washington State University
Pullman, WA 99164-2814

Jermaine L. Kennedy
and Joseph L. Lopes
Naval Surface Warfare Center
Panama City Division
Panama City, FL 32407-7001

Abstract—A series of monostatic and bistatic acoustic scattering measurements were conducted to investigate discrimination and classification capabilities based on the acoustic response of targets for underwater unexploded ordnance (UXO) applications. The measurements were performed during March 2010 and are referred to as the Pond Experiment 2010 (PondEx10), where the fresh water pond contained a sand sediment. The measurements utilized a rail system with a mobile tower and a stationary sonar tower. Each tower is instrumented with receivers while the sources are located on the mobile tower. For PondEx10, eleven targets were deployed at two distinct ground ranges from the mobile tower system. Acoustic data were initially processed using synthetic aperture sonar (SAS) techniques, and the data were further processed to generate acoustic templates for the target strength as a function of frequency and aspect angle. Preliminary results of the processing of data collected from proud targets are presented. Also presented are the results associated with a processing technique that permits isolation of the response of an individual target, which is in close proximity to other targets.

I. INTRODUCTION

Although the practice of disposing conventional and chemical munitions in coastal waters was discontinued during the 1970's, the environmental, economical, and even the recreational impact persists today [1]. In Overfield and Symons' overview of the Resources and UnderSea Threats (RUST) database [2], they note that 2100 underwater sites are likely to contain munitions. Of those 2100 sites, verification has been completed on only slightly more than 50%. Schwartz and Brandenburg [3] summarize the current technologies available for underwater UXO applications. Their Table 1 includes metal detection (e.g., electromagnetic induction and magnetometers), chemical sensors (spectroscopy and fluorescence), and sonar. Metal detection and chemical sensors are typically restricted to short ranges; while the sonar technologies considered are limited in range (e.g., Didson system) or are limited by poor penetration into sediments (e.g., side-scan sonar) due to the high frequencies used. Furthermore, Schwartz and Brandenburg note that SAS is still a relatively new technology in UXO detection and that low-frequency SAS systems have demonstrated detection of proud and partially buried objects [4].

Low-frequency SAS systems with a wide bandwidth have several advantages over higher frequency sonar systems. Low

frequencies offer greater detection ranges, which permits the surveying of wider areas. In addition, low frequencies attain greater penetration depths into sediments, which permit detection of partially and completely buried munitions. The range resolution of a SAS system is related to the bandwidth of the transmitted signal where a wider bandwidth provides higher resolution. Thus, we report here on our preliminary analysis of UXO detection and discrimination by a low-frequency wide bandwidth SAS system. Our work compliments that of Bucaro *et al.* [4] in that they consider isolated UXO in their research. The experiments conducted during PondEx10 have multiple UXO in the field of view of the SAS system with a minimum separation distance of 1.5 m.

II. POND EXPERIMENT 2010

PondEx10 was carried out in a fresh water pond located at the Naval Surface Warfare Center, Panama City Division (NSWC PCD). This pond holds approximately 9 million gallons of water, and has nominal dimensions of 110 m in length and 80 m in width. The water depth at the location of the deployed target fields is ~ 14 m. A ~ 1.5 m thick layer of medium-fine sand covers the bottom of pond. To prevent biological growth and fouling of the targets and equipment, the water is filtered and chlorinated. During the PondEx10 exertions, the sound speed in the water, which was determined from temperature measurements acquired from the divers, was found to be 1456 m/s. A detailed drawing and aerial view of the pond can be found in [5].

Eleven targets were deployed in the measurements. The targets included a solid aluminum cylinder, an aluminum pipe, an inert 81 mm mortar (filled with cement), a solid steel artillery shell, two machined aluminum UXO, a machined steel UXO, a de-militarized 152 mm TP-T round, a de-militarized 155 mm empty projectile (without fuse or lifting eye), a small aluminum cylinder with a notch, and two rocks with sizes comparable to the UXO targets. Figure 1 shows a few of the UXO and generic shapes used. The machined UXO, based on a CAD drawing of the solid steel artillery shell, were constructed from materials with known properties. The aluminum cylinder is 2 ft long with a 1 ft diameter; while the pipe is 2 ft long with an inner diameter of 1 ft and 3/8 inch wall thickness.



Fig. 1. A selection of targets used during PondEX10. From left to right, the targets are a machined aluminum UXO, solid steel artillery shell, small aluminum cylinder with a notch, de-militarized 152 mm TP-T round, 81 mm mortar, and de-militarized 155 mm UXO. Rock 2 is in the foreground.

A rough layout of the 10 m target field is illustrated in Fig. 2. Divers first deployed a 21 m long rail system, which consists of three independent sections (see Fig. 1 in [5]). The sections are connected and leveled to establish a baseline for the geometry of the experiment. The divers then surveyed in two screw anchors at an 11 m ground range from the rail, where the dashed lines in Fig. 2 depict temporary lines for placing the left screw anchor. A lightweight guide line is then stretched between the screw anchors and marked at 4, 7, 10, 13, and 16 m from the left screw anchor. These locations are enumerated as Target Patch #1 through #5, and mark the sites of 1 m² patches, where targets are deployed (dark blue patches in Fig. 2). When seven targets are present, the additional two targets are placed in 1 m² patches between Target Patches #2 and #3 and Target Patches #3 and #4 (light blue patches in Fig. 2).

Target Patches were created by the divers using a set of T-bar aluminum rails that are registered against the 11 m guide line. One T-bar aluminum rail, referenced to the guide line, is driven into the sediment while the second rail is placed meticulously parallel with the first T-bar with a separation distance of ~ 1 m. The second T-bar is then driven into the sediment, and the rails are checked for levelness. Divers smooth the sand interface by scraping a third aluminum bar, which is perpendicular to the two T-bar rails, along these rails. Low spots, if observed, are filled with sand from outside the target field. This procedure is followed prior to a set of measurements, where the targets are rotated through a set of orientations (relative to rail).

To orient the targets, a square PVC frame with dimensions comparable to the target patch is utilized. One side of the frame is referenced to the 11 m guide line, which enables all four sides of the frame to encompass a Target Patch. A series of holes in the frame allowed the divers to select one of several angles. The angles used in PondEX10 for targets

with cylindrical symmetry ranged from -80° to 80° in 20° increments. A target is broadside to the rail system at 0° with the nose of a UXO pointing towards a stationary tower. The nose (tail) of a UXO pointed towards the rail in the -80° (80°) orientation. For the rocks, the rotations covered -80° to 260° due to their asymmetry.

The mobile tower is placed on the rail system, and it holds acoustic sources and receivers. The mobile tower moves at 0.05 m/s with the source transmitting a ping every 0.5 s. The total distance traveled along the rail is 19 m. Thus, a SAS data set contains 760 pings, and each data set is referred to by a “sequence number”. The receiver on the mobile tower is a six channel vertical array, where each channel is recorded separately at a 1 MHz sample rate. The acoustic receivers located on the stationary sonar tower (see Fig. 2) were mounted on horizontal pan and vertical tilt motors, which allowed accurate alignment of the main lobe of the receivers with the Target Patches. The stationary receivers recorded data at a 500 kHz sample rate. The sources and receivers on both the rail system and stationary sonar tower stood about 4 m above the water-sand interface. When traveling from left-to-right in Fig. 2, the source transmitted a 6 ms LFM chirp centered at 16 kHz with 30 kHz of bandwidth. On the return trip, the source transmitted a 4 ms LFM chirp centered at 40 kHz with 20 kHz of bandwidth.

Two target fields were deployed during the course of PondEX10: one with targets at 10 m ground range from the rail system and one with targets at 5 m ground range. At a 10-m ground range, the targets were proud on a flattened water-sand sediment interface; while the targets were either proud, half-buried, or flush buried when placed at 5 m. The 10 and 5 m ranges correspond to $\sim 20^\circ$ and $\sim 40^\circ$ grazing angles with respect to the source and receiver locations, respectively. The critical grazing angle for the sand sediment in the test pond was nominally 28° . Thus, data collected for the proud targets were at shallow and steep grazing angles; while data collected for the half-buried and fully buried targets corresponded to a steep grazing angle case. When five targets were placed in the target field, the separation distance between adjacent targets was approximately 3 m. This distance was selected to minimize multiple scattering between targets. When the additional two targets were inserted into the target field, the separation distance was reduced to 1.5 m for the inner five targets.

III. DATA PROCESSING AND DISCUSSION

The data were initially processed using time-domain and frequency-domain synthetic aperture sonar (SAS) techniques in which high resolution images were generated. A brief description of the time-domain method follows. First, a raw SAS data set is pulse compressed by match filtering the pings with a replica of the transmitted LFM chirp. During the match filtering, a Hilbert transform converts the real-valued recorded pings to complex-valued signals. Next, baseband pulse-compressed data is obtained by removing the carrier

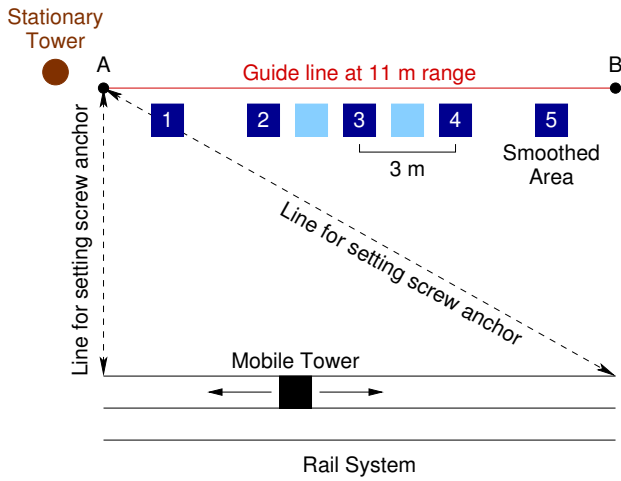


Fig. 2. Schematic layout of the target field. The left and right screw anchors are denoted by 'A' and 'B'.

frequency, i.e., multiplying by $\exp(i\omega_0 t)$, where ω_0 is an angular carrier frequency and our processing scheme assumes a negative time convention. Figure 3 shows the magnitude of the baseband pulse-compressed pings for sequence 27, which used the 1–31 kHz LFM chirp. This sequence included (from top to bottom in Fig. 3) the machined aluminum UXO #1, 2:1 solid aluminum cylinder, machined steel UXO, 2:1 aluminum pipe, and the solid artillery shell in a proud, broadside orientation. It is immediately evident that the scattered acoustic field from the individual targets interfere with their neighbors. The overlap of the scattered acoustic fields has an important consequence for the acoustic template processing discussed below. However, for SAS processing the coherent addition of the complex time signals is unaffected by this overlap. The next step to produce a SAS image from the time-domain data is to use a simple delay-and-sum beamformer [6]. For each pixel in a SAS image, the signals are time shifted to account for propagation from the source to the pixel and then from the pixel to the receiver. Once the time shift is performed, the signals are coherently added to determine a complex reflectivity of the pixel. This time shifting is done for each pixel in a SAS image. Images for individual channels of the receive array as well as the superposition of the six channels have been constructed.

SAS images for the targets in sequence 27 are shown in Fig. 4. These images are $1 \times 2 \text{ m}^2$ patches with a 1 cm^2 resolution, where the six channels of the receive array have been summed. The relative dB scale is determined from the magnitude of the “hottest” pixel with the two-way spreading loss removed.

Figure 3(a) in [5] is a SAS image of the same solid aluminum cylinder obtained in the previous year’s PondEx09 measurement, and it is similar to Fig. 4(b) shown here. Williams *et al.* developed an acoustic ray model (see Fig. 5 in [5]) to understand the observed triplet structure. Briefly, the rays that contribute to this structure are: (1) a specular ray directly reflected from the cylinder; (2) a ray reflected from the cylinder that then reflects from the water-sand interface;

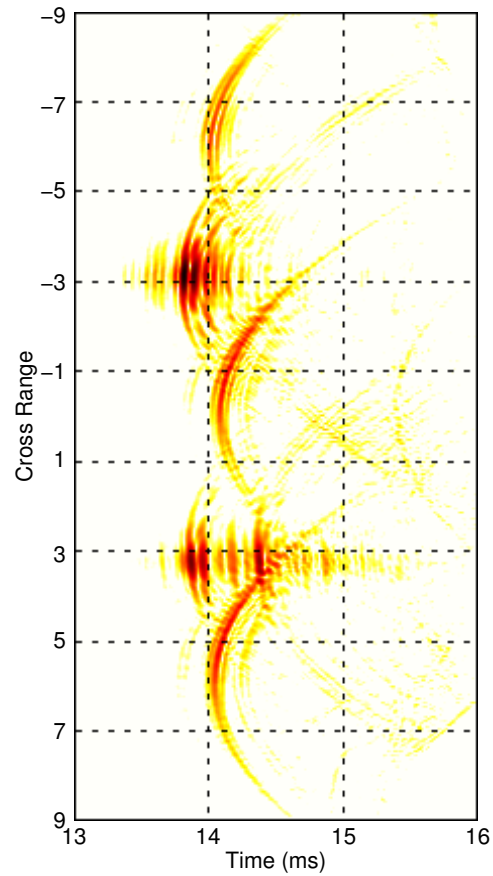


Fig. 3. Baseband pulse-compressed data for sequence 27. The image is normalized by the maximum value in the data and displayed on a 0 to –30 dB color scale.

(3) a ray reflected from the water-sand interface that reflects from the cylinder; and (4) a ray reflected from the water-sand interface reflects from the cylinder and then follows its incoming path to reflect once again from the sediment. The features beyond the triplet structure has been associated with the elastic response of the target.

The geometric shape of the targets in Figs. 4(a), (c), and (e) are identical. In Fig. 4(a), the triplet structure observed with the solid cylinder is again seen. Given the cylindrical symmetry of these targets, it is not unexpected to observe a similar structure. The triplet structure is not observed in (c) and (e). This may be a consequence of the “brightness” of the steel targets, the small time difference in the arrival of the four ray paths to the receiver, and the 20 dB range used to display the image. Comparison of these images also shows that the aluminum target has a much weaker feature following the main geometric response. This suggests over the frequency range of the LFM chirp, the machined aluminum UXO has a much different elastic response in comparison to the machined steel UXO and the solid steel artillery shell. Finally, in (c) the feature near 10.75 m is due to a screw anchor that was inadvertently left in the target field during the collection of sequence 27.

The final SAS image to consider is that of the aluminum

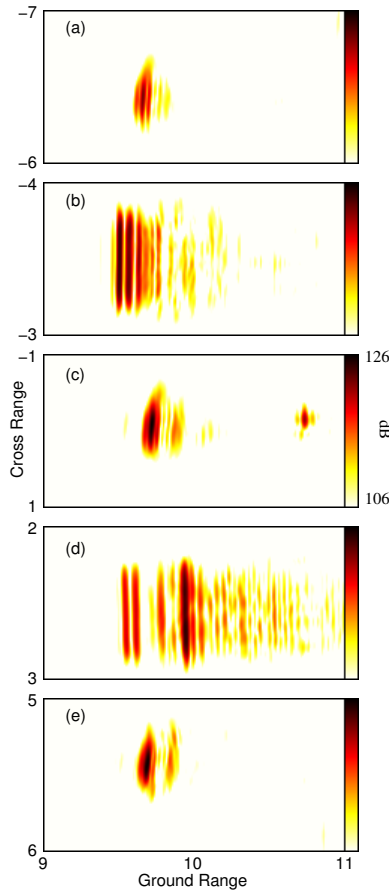


Fig. 4. SAS images of the targets in for sequence 27: (a) machined Al UXO #1, (b) solid Al cylinder, (c) machined steel UXO, (d) Al pipe, and (3) solid artillery shell.

pipe in Fig. 4(d). The triplet structure is no longer found and instead a doublet appears. A physical acoustics based ray model has yet to be constructed. Presumably, one or more reflection coefficients needed in the ray models for the water-filled cylindrical shell may lead to a destructive interference of some of the ray paths. The bright return at 10 m is associated with an acoustic field that is transmitted into the pipe and reflected from the far side. The other observed structure probably is due to an elastic response of the pipe. Finite element modeling of this experimental situation is an on-going task.

The data were further processed to generate acoustic templates of the target strength as a function of frequency and aspect angle. Due to the relatively small separation distances between the UXO targets, the scattered fields from the targets overlap (see Fig. 3). To generate an acoustic template, a novel SAS filtering technique was used to isolate the response of an individual target and to suppress reverberation noise. The details of the SAS filtering will be given elsewhere. A brief summary is as follows. The raw SAS data set is deconvolved with a target arc (i.e., point spread function) for a single selected location in an image plane, and a SAS image is formed. As an observation point in the SAS image moves

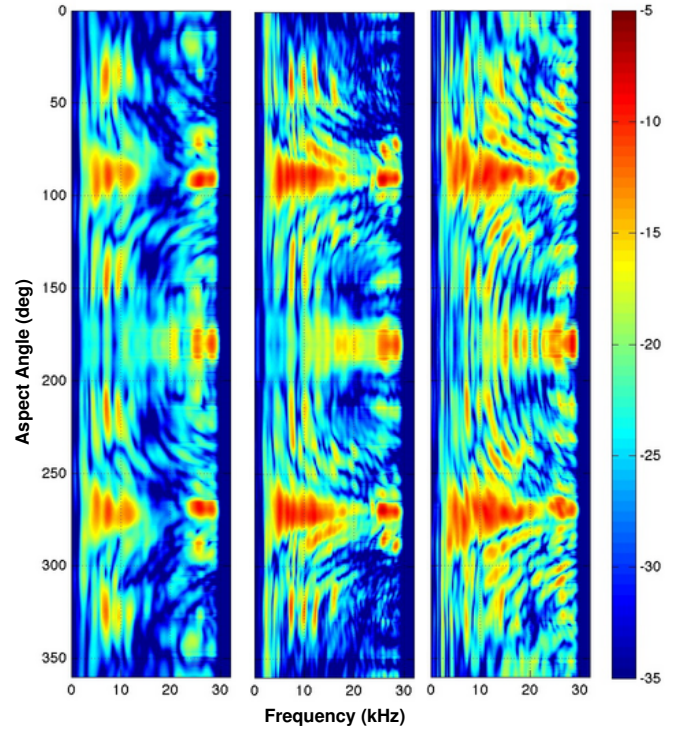


Fig. 5. Acoustic template for for the machined Aluminum UXO #1 (left), machined steel UXO (center), and (3) solid steel artillery shell (right).

away from the selected location, the image becomes defocused because the target arc is not appropriate for distant locations. The SAS image is then windowed in the spatial domain about the selected location. This windowed image contains the information to reconstruct the time signals associated with a given target via a convolution with the same target arc. It is noteworthy that the deconvolution and convolution processes are linear operations, and hence in the absences of multiple scattering the recovered signal isolates the response of the selected target.

Inspection of the target arcs in Fig. 3 suggests that, at most, an aspect angle range for a given target in a given sequence spans approximately $\pm 15^\circ$. This motivated the choice of target rotations from -80° to 80° in 20° increments. Thus, adjacent rotation angles provide an overlap in the aspect angle ranges (e.g., $20^\circ \pm 15^\circ$ and $40^\circ \pm 15^\circ$), which permits the nine sequences to be stitched together to form the acoustic templates in Fig. 5. The overlapping regions were determined by a cross-correlation of the aspect angle ranges for adjacent rotation angles. Once the overlap was established, the two ranges are merged by a smoothing operation over the overlap region.

A cursory inspection of Fig. 5 reveals that the structure observed for the machined steel UXO is a better match to the steel artillery than the machined aluminum UXO. In this figure, 90° and 270° correspond to a broadside orientation, 0° and 360° have the nose of the ordnance pointing at the rail system, and 180° corresponds to the tail pointing toward the

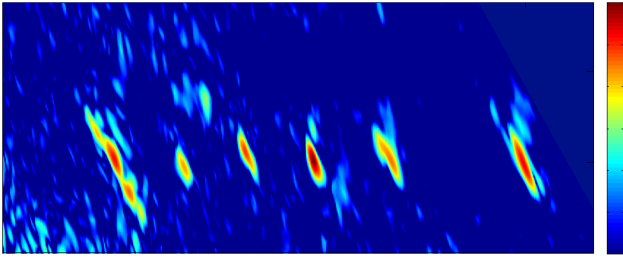


Fig. 6. Bistatic SAS image for sequence 258.

rail. Currently, finite element models of these UXO are being constructed to investigate the observed acoustic templates. Based on the results of Williams *et al.* and Bucaro *et al.*, it is anticipated the observed differences are associated with the elastic response of the target [4], [5].

Figure 6, generated from sequence 258, is an example of the bistatic images generated by processing data using SAS methods. The source on the mobile tower rail system transmitted an acoustic signal, which was a 4 ms LFM chirp with a 40 kHz carrier frequency and 20 kHz bandwidth. While it traveled the length of the rail, the receivers on the stationary tower were utilized to record the scattered signals for six targets in the field 10 m from the mobile tower. This sequence included (from left to right) the 152 mm TP-T round, aluminum cylinder with notch, solid steel artillery shell, inert 81 mm mortar (filled with cement), machined aluminum UXO #1, and the 155 mm empty projectile. These targets were all in a proud configuration oriented at 40° with respect to the mobile tower rail system. The image reveals the target separation for the first five targets (from left to right) were ~ 1.5 m corresponding to the minimum separation distance examined during PondEx10; while the last target had a separation distance of 3 m from the fifth target. In this image the color scale corresponds to a logarithmic scaling of the scattered intensity relative to the image maximum over a 30 dB range. Interpretations harvested from a host of bistatic sequences acquired during these experiments are currently being processed with the intentions of implementing additional finite element modeling to explain and decipher the results.

IV. CONCLUSION

The preliminary analysis of PondEx10 SAS data sets suggest that low frequency wide bandwidth SAS systems are capable of UXO detection and discrimination. Work remains to demonstrate that the acoustic template for a given UXO can be used as a fingerprint to uniquely identify a detected target as a UXO. The results of a finite element model analysis of the solid cylinder and partial results for the pipe have shown the complex structure found in their acoustic templates can be directly related to an elastic response of the target. Finite element models for the various UXO in our experiments are currently under investigation, where it is anticipated that the structure observed in Fig. 5 may be reproduced. Finally, the current method for the construction of the acoustic templates demonstrates that the SAS filtering technique and the merging of aspect angle ranges via correlation and smoothing techniques provide a robust approach to acoustic template generation.

ACKNOWLEDGMENT

Partial support was provided by The Strategic Environmental Research and Development Program (SERDP) under projects MM-1665 and MM-1666 and by the Office of Naval Research.

REFERENCES

- [1] Terrence P. Long, "A global perspective on underwater munitions," *Mar. Technol. Soc. J.*, **43**, 5–10 (2009).
- [2] Mike L. Overfield and Lisa C. Symons, "The use of the RUST database to inventory, monitor, and assess risk from Undersea Threats," *Mar. Technol. Soc. J.*, **43**, 33–40 (2009).
- [3] Andrew Schwartz and Erika Brandenburg, "An overview of underwater technologies for operations involving underwater munitions," *Mar. Technol. Soc. J.*, **43**, 62–75 (2009).
- [4] J. A. Bucaro, B. H. Houston, M. Saniga, L. R. Dragonette, T. Yoder, S. Dey, L. Kraus, and L. Carin "Broadband acoustic scattering measurements of underwater unexploded ordnance (UXO)," *J. Acoust. Soc. Am.*, **123**, 738–746 (2008).
- [5] Kevin L. Williams, Steven G. Kargl, Eric I. Thorsos, David S. Burnett, Joseph L. Lopes, Mario Zampolli, and Philip L. Marston, "Acoustic scattering from a solid aluminum cylinder in contact with a sand sediment: Measurements, modeling, and interpretation," *J. Acoust. Soc. Am.*, **127**, 3356–3371 (2010).
- [6] Steven G. Kargl, Kevin L. Williams, Eric I. Thorsos, and Joseph L. Lopes, "Bistatic synthetic aperture sonar measurements and preliminary analysis," in *Boundary Influences in High Frequency, Shallow Water Acoustics*, N. G. Pace and P. Blondel (Eds.), University of Bath, UK, Sept., 2005, pp. 137–143.